

THE KINETICS AND MECHANISM OF CATALYTIC REACTIONS BY MOLECULAR BEAM RELAXATION SPECTROSCOPY: HCOOH DECOMPOSITION

Israel E. WACHS and Robert J. MADIX

Department of Chemical Engineering, Stanford University, Stanford, California 94305, USA

Received 26 April 1976; manuscript received in final form 27 December 1976

The reactive scattering of formic acid from Ni(110) was studied over the temperature range of 175–920 K with MBRS in the millisecond time region by employing a modulation frequency of 36.8 Hz. The steady-state carbon and oxygen composition of the surface varied over the range of temperatures studied. For beam fluxes of 10^{13} molecules/cm² sec the onset of decomposition on the steady-state surface occurred at 300 K. By 400 K decomposition was essentially complete, and the products CO₂, CO, H₂ and H₂O were detected. All reaction events were preceded by a common step, and the products were then produced by a series/parallel mechanism. The rate constants measured for H₂ and H₂O formation indicated stringent limitations on the efficiency of second-order collisions on the surface for producing gaseous products. This study illustrates the use of MBRS for surface reaction mechanistic studies in the millisecond time scale.

1. Introduction

The application of molecular beam relaxation spectrometry (MBRS) to the study of high temperature heterogeneous reactions has led to the identification of several types of reaction processes occurring on solid surfaces [1–5]. The utility of MBRS in studying fundamental reaction steps in heterogeneous reactions rests on the fact that reaction products formed on the surface can be modulated to probe the characteristic reaction times of the individual steps. In this work we have studied the steady-state decomposition of formic acid on a Ni(110) surface in order to (1) assess the general utility of MBRS for mechanistic studies, (2) determine the characteristics of this specific reactive scattering event in order to compare the temperature-steady-state MBRS behavior to that observed in flash desorption studies [6–9].

The techniques of flash desorption and MBRS provide complementary information for describing the dependence of surface reactions on temperature, pressure and surface coverage. The primary difference in the two methods is the steady-state temperature and the lower coverages employed in MBRS. The mode of operation in MBRS allows reactions to be studied at temperatures well above the temperatures

at which one or more reactants might be desorbed under flash desorption conditions so that interactions between them could not be observed.

As a result of these differences the combined use of MBRS and flash desorption presently provides for the study of the kinetics and mechanism of surface reactions for surface coverages ranging from 10^{-4} to 1.0 monolayers of adsorbed gas and for characteristic reaction times ranging from 10^{-5} to 10 sec. As shown below, MBRS can be utilized to trace the reactive scattering behavior of the reactant from temperatures too low to produce reaction to temperatures at which reaction is essentially complete. This quantitative capability should make extensive studies of the kinetics and mechanism of catalytic reactions on single-crystals feasible.

2. Experimental

A detailed description of the ultra-high vacuum chamber and the reagents used in this study has been published elsewhere [9]. The experiments reported here were performed utilizing a UTI quadrupole mass spectrometer. As shown in fig. 1, the UHV chamber was equipped with a modulated molecular beam system, a PHI four-grid LEED-Auger optics, an argon ion bombardment gun, and the mass spectrometer. The base pressure of the UHV system was usually about 2×10^{-10} Torr and

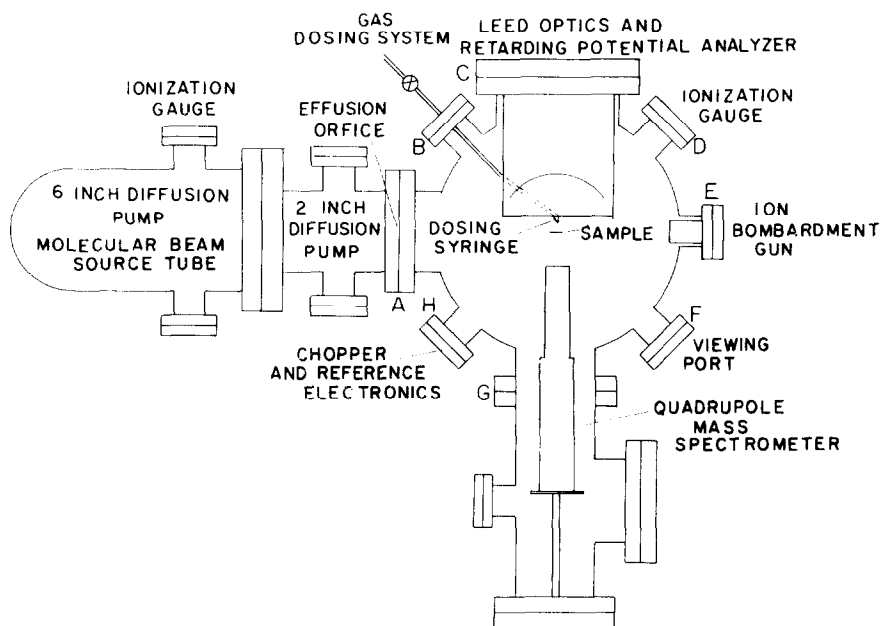


Fig. 1. Top view of ultra high vacuum MBRS chamber.

increased to the low 10^{-9} Torr range when the molecular beam was operating. Both the flux of the HCOOH molecular beam at the Ni(110) surface and the modulation frequency were kept constant throughout the experiment at approximately 10^{13} molecules/cm²sec and 36.8 Hz, respectively.

The molecular beam was generated in an array of fused capillaries of 0.005 cm diameter and was collimated by a 2 mm hole located in a solid copper gasket that separated the beam source from the main chamber. Another collimator, not shown in the schematic, was placed between the effusion orifice and the Ni(110) single crystal sample. Alignment of the molecular beam was achieved with a 120 mW helium–neon laser beam. The sample and the mass spectrometer were separated by approximately 4 cm in order to minimize the transit time. The surface normal of the crystal was held at approximately 45° from both the effusion orifice and the mass spectrometer. The molecular beam was modulated by a balanced three-bladed aluminium disk located inside the main chamber. The reference signal was generated by placing a photodiode and a small bulb on opposite sides of the chopper blade. The transit time of the system was determined by measuring the phase-lag for a molecular beam of argon.

The ac mass spectrometer signal was monitored by a phase-sensitive detector and a waveform eductor. An Ithaco Dynatrac 391A lock-in amplifier was used for phase-sensitive detection, and a PAR TDH-9 waveform eductor was used to obtain the relaxation spectrum. Since the ac signal to noise ratio was large it was only necessary to use a 1.25 sec time constant for the phase-sensitive detector. The waveforms were first examined on an oscilloscope and then plotted on an X–Y recorder. Typical time constants used in storing the product response curves ranged from 20 to 50 sec.

Surface cleanliness was achieved at the beginning of each experiment by argon ion sputtering and annealing and was verified by Auger electron spectroscopy. A surface carbon monolayer was defined as the saturation carbon coverage obtained from cracking ethylene at saturation coverage on the nickel surface; a coverage of 1.1×10^{15} oxygen atoms/cm² was defined as a surface oxygen monolayer [10].

In order to obtain a better understanding of the influence that catalysts have upon chemical reactions it was necessary to have information about the state of the surface of the catalyst during the reaction. The steady-state composition of the Ni(110) surface during the reaction was determined by AES after an exposure of 30 min to $\sim 1 \times 10^{-7}$ Torr of formic acid at a series of temperatures. The surface compositions are presented in table 1 for the different temperatures investigated. Substantial amounts of carbon and oxygen accumulated on the Ni(110) surface between 400–600 K. No carbon was observed above 665 K, and no oxygen was observed above 830 K; the surface was essentially clean at higher temperatures.

The nickel surface was free of carbon and oxygen at elevated temperatures because at these temperatures adsorbed carbon and oxygen readily reacted to form gaseous carbon monoxide [9,11]. The temperature of the surface having the composition shown at 465 K in table 1 was subsequently increased to 665 K without

Table 1

AES analysis of the steady-state surface coverage of Ni(110) after 30 min exposure to formic acid

| Catalyst temperature (K) | Carbon coverage (fraction of a monolayer) | Oxygen coverage (fraction of a monolayer) |
|--------------------------|---|---|
| 407 | 0.19 | 0.27 |
| 465 | 0.28 | 0.34 |
| 665 | ~0 | 0.30 |
| 760 | ~0 | 0.18 |
| 830 | ~0 | ~0 |

exposing the sample to formic acid; after 30 min the surface showed no traces of carbon or oxygen by AES analysis. In addition, ~0.60 monolayer of carbon was deposited on the nickel surface at 465 K; after exposing the surface to formic acid for 30 min at 665 K the carbon content decreased significantly, but no oxygen AES signal was observed.

The change in the steady-state surface composition with temperature gave rise to a hysteresis in the rate of production of the reaction products. Since the decomposition probability of formic acid depended on the amount of surface carbon (and therefore so did the quantity of product formed), the manner in which the data was collected was important. Fig. 2 shows the amplitude behavior of the $\text{CO}_2/\text{DCCOOH}$

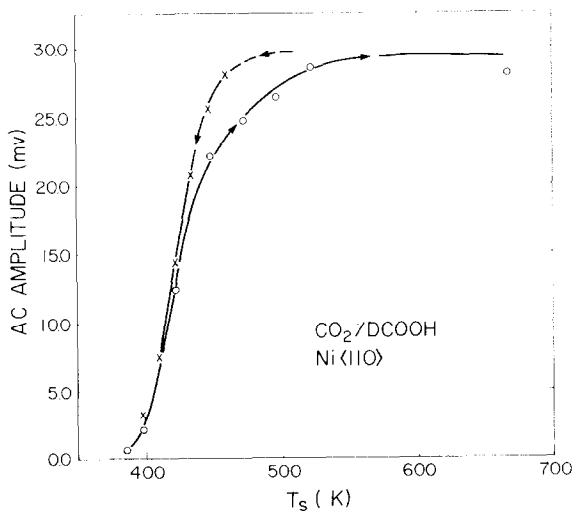


Fig. 2. Hysteresis in the rate of CO_2 production due to the temperature dependence of the Ni(110) steady-state surface composition; (○) increasing surface temperature; (X) decreasing surface temperature.

DCOOH as the substrate temperature was increased from 385 to 668 K, and subsequently decreased. After approximately 10–15 min of operation in the temperature range 400–500 K, the higher activity was lost because of carbon accumulation on the surface.

Since the nickel surface was clean at high temperatures the data for the *product* species was normally collected by starting at the highest surface temperature. The data for the desorption of formic acid itself was obtained by starting at the lowest surface temperature. This procedure was used in order to keep the nickel surface relatively free of carbon throughout most of the experiment, and to obtain reproducible experimental results.

The CO signal was corrected for contributions from cracking fractions of HCOOH and CO₂ in the mass spectrometer. The H₂O signal also was corrected for a small amount of H₂O that formed from ions in the mass spectrometer. These corrections were achieved by utilizing the equations for a branched process presented below.

3. MBRS analysis

The data from the modulated molecular beam experiments was analyzed either by phase-sensitive lock-in detection [12,13] (which utilized the phase-lag and amplitude of the first harmonic of the response function) or by direct examination of the relaxation spectrum [14,15]. In the case of a simple adsorption–desorption process *not undergoing a chemical transformation* and being forced by a square pressure pulse of molecules that have an adsorption probability of unity on the solid surface, the desorption rate, R , is:

$$R_{\text{beam on}} = R_{\text{ss}}(1 - C_{\text{on}} e^{-kt}), \quad (1)$$

$$R_{\text{beam off}} = R_{\text{ss}}(C_{\text{off}} e^{-kt}), \quad (2)$$

where R_{ss} is the steady-state desorption rate in the absence of modulation, k is the first-order rate constant for desorption, C_{on} and C_{off} are constants that are independent of time, and t is the time elapsed from the moment the beam is turned on or off, respectively. The waveform for such a first-order process behaves exponentially; the rate constant is therefore easily determined if the waveform can be accurately measured. The corresponding lock-in phase-lag and amplitude for this process are:

$$\phi = \tan^{-1}(\omega/k), \quad (3)$$

$$S \propto \frac{I_0}{[1 + (\omega/k)^2]^{1/2}}, \quad (4)$$

where I_0 is the intensity of the molecular beam expressed in units of molecules/cm²sec, and ω is the modulation frequency in radians/sec ($\omega = 2\pi f$).

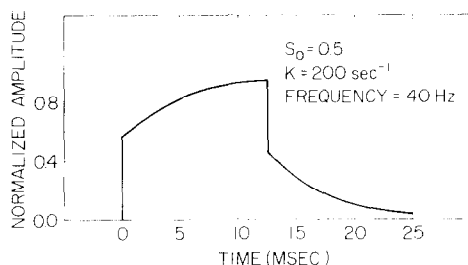


Fig. 3. Response function for an initial square pressure pulse of molecules that were simultaneously reflected and adsorbed with a finite surface residence time.

The deviation of the adsorption probability from unity appears as a discontinuity in the waveform (shown in fig. 3). The discontinuity occurs because a portion of the incident molecules are instantaneously reflected, while the remaining molecules undergo a first-order process and, as a result, desorb exponentially. The adsorption probability, s_0 , can be calculated from the discontinuity in the waveform. Under these circumstances the lock-in expressions for the phase-lag and amplitude are:

$$\phi = \tan^{-1} (B/A), \quad (5)$$

$$S \propto (A^2 + B^2)^{1/2} I_0, \quad (6)$$

$$A = (1 - s_0) + \frac{s_0}{1 + (\omega/k)^2}, \quad (7)$$

$$B = \frac{s_0(\omega/k)}{1 + (\omega/k)^2}. \quad (8)$$

Eqs. (5) and (6) reduce to eqs. (3) and (4) when s_0 approaches unity.

Some reactions may simultaneously produce the same product by two different mechanisms. On a heterogeneous surface (containing more than one type of site) the relative importance of the two paths *subsequent to adsorption* is represented by the branching probability, P , which may be related to the relative abundance of the different sites. For a chemical reaction occurring on a heterogeneous surface, for example, having two parallel paths with rate constants k_1 and k_2 , the phase-lag and amplitude are given by eqs (5) and (6) and A and B are now given by [13]

$$A = \left[\frac{P}{1 + (\omega/k_1)^2} + \frac{1 - P}{1 + (\omega/k_2)^2} \right] s_0, \quad (9)$$

$$B = \left[\frac{P(\omega/k_1)}{1 + (\omega/k_1)^2} + \frac{(1 - P)(\omega/k_2)}{1 + (\omega/k_2)^2} \right] s_0. \quad (10)$$

Bernasek and Somorjai have observed such a process in the exchange of H_2 and D_2

on stepped platinum surfaces [16]. On a homogeneous surface (containing only one type of site) the relative importance of the two paths is determined by the relative resistances toward product formation. The equations for a branched process on a homogeneous surface are identical to those for a simple adsorption-desorption process previously presented (eqs. (3) and (4)), except that the first order rate constant, k , is replaced by $k_1 + k_2$, the rate constants for the parallel branches.

The exact expressions for the amplitude and phase-lag of a second-order surface process were recently derived by Olander and Ullman [17]. Schwarz and Madix derived similar expressions using linearization techniques [2]. The exact expressions due to Olander et al. are

$$\phi = \tan^{-1} \left(\frac{\omega}{[2s_0 I_0 (1 + 1/\epsilon) k_2]^{1/2}} \right), \quad (11)$$

$$S \propto \frac{s_0 I_0}{[1 + \omega^2 / 2s_0 I_0 (1 + 1/\epsilon) k_2]^{1/2}}, \quad (12)$$

where k_2 is the second-order rate constant and ϵ is the ratio of beam to background supply rates. If s_0 and I_0 are maintained constant the above equations for a second-order process are indistinguishable in form from those of a first-order process (eqs. (3) and (4)). For a second-order rate constant with a pre-exponential factor A_2 and an activation energy E , the apparent first-order rate constant is:

$$k_{\text{app}} = A_{\text{app}} \exp(-E_{\text{app}}/RT), \quad (13)$$

$$A_{\text{app}} = [2s_0 I_0 (1 + 1/\epsilon) A_2]^{1/2}, \quad (14)$$

$$E_{\text{app}} = E/2. \quad (15)$$

A series mechanism can exhibit a phase-lag that exceeds 90° . For a series mechanism consisting of two steps with rate constants k_1 and k_2 , each step contributes to the phase-lag and amplitude demodulation; therefore,

$$\phi = \tan^{-1} (\omega/k_1) + \tan^{-1} (\omega/k_2), \quad (16)$$

and

$$S \propto \frac{s_0 I_0}{[1 + (\omega/k_1)^2]^{1/2} [1 + (\omega/k_2)^2]^{1/2}}. \quad (17)$$

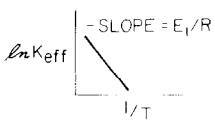
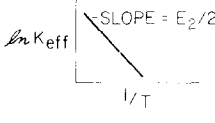
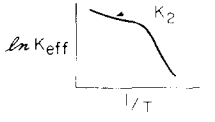

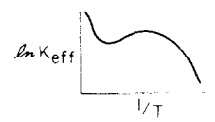
Each of the different reaction mechanisms discussed above shows unique distinguishing features. Examination of the lock-in phase-lag data (ϕ) at a series of substrate temperatures (T) at a single modulation frequency provides a straightforward approach for distinguishing the different reaction mechanisms. In addition, for most of the mechanisms encountered in MBRS all of the kinetic parameters may be

directly deduced from the ϕ versus T data. For more complicated mechanisms, however, a determination of the dependence of the phase-lag and amplitude on frequency is necessary before all of the kinetic parameters can be determined. To distinguish between the different types of reaction mechanisms it is necessary to plot the effective rate constant, defined by

$$k_{\text{eff}} = \omega / \tan \phi \quad (18)$$

in an Arrhenius fashion. Table 2 shows that each type of surface reaction exhibits its own unique features when examined this way. The first-order and second-order reactions show similar behavior, but the second-order reaction can be easily distinguished by the dependence of the phase-lag on the beam intensity [2]. For both first and second-order processes, the kinetic parameters are directly determined from the Arrhenius plot. The series process and each of the two parallel processes have clear and unique distinguishing features that are easily identifiable. Both the series process and the parallel process for a homogeneous surface allow for the

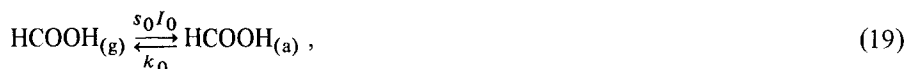
Table 2

| Reaction mechanism | k_{eff} | Arrhenius plot ($E_1 > E_2$) |
|-------------------------------------|--|---|
| First order | k_1 |  |
| Second order | $[2s_0 f_0 (1 + 1/\epsilon) k_2]^{1/2}$ |  |
| Series | $\frac{k_1 k_2}{k_1 + k_2}$ |  |
| Parallel (homogeneous surface) | $k_1 + k_2$ |  |
| Parallel (heterogeneous surface) | $\frac{P(\omega/k_1)}{1 + (\omega/k_1)^2} + \frac{(1-P)\omega/k_2}{1 + (\omega/k_2)^2}$ $\frac{P}{1 + (\omega/k_1)^2} + \frac{1-P}{1 + (\omega/k_2)^2}$ |  |

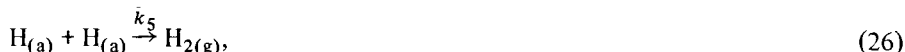
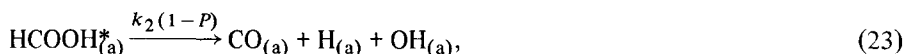
direct calculation of all the kinetic parameters (see table 2). Once one of the rate constants is determined, the second rate constant is directly calculable. For the parallel process on a heterogeneous surface the three kinetic parameters (P , k_1 , and k_2) are not directly accessible and frequency variation data is necessary before these parameters can be calculated. Unfortunately, in the limit where the two rate constants k_1 and k_2 have very similar activation energies and pre-exponentials, the series and parallel processes become indistinguishable from the simple first-order process. In such a case frequency variation at different temperatures may help to dissect the mechanism.

4. Results

The data presented below for the interaction of an HCOOH molecular beam with a Ni(110) surface suggested the following surface process below room temperature:



where $\text{HCOOH}_{(a)}$ represents the physisorbed formic acid and $\text{HCOOH}_{(a)}^*$ represents the chemisorbed formic acid. Below room temperature the surface was saturated with chemisorbed formic acid. At elevated temperatures the concentration of reaction intermediates on the Ni(110) surface was very low and the following mechanism prevailed:



where P is the probability that formic acid decomposed to CO_2 , and $1 - P$ is the probability that CO was formed. The details of this mechanism are discussed in detail below.

4.1. Adsorption-desorption of HCOOH

The temperature dependence of the amplitude of the desorbing formic acid molecules and the decomposition products appears in fig. 4. Below 300 K the amplitude of the formic acid signal decreased with decreasing surface temperature as a result of signal demodulation; above 300 K the amplitude decreased with increasing surface temperature because of decomposition. The amplitude attenuation due to reaction exceeded 90% at 380 K and decreased to 80% as the temperature approached 500 K. The formation of surface carbon in this temperature range appeared to be responsible for this decrease in the decomposition probability. The amplitudes for the reaction products (CO_2 , CO , H_2O and H_2) shown in this figure were not corrected for the mass spectrometer sensitivities of the different species. At 400 K most of the formic acid was decomposed, and the modulated signals of the reaction products began to appear. Above 700 K a change in selectivity was observed in the relative formation of product species as marked by the sharp decrease in the CO_2 signal.

The flash desorption spectra following HCOOH adsorption on a Ni(110) surface at approximately 150 K to high coverage revealed two binding states for HCOOH

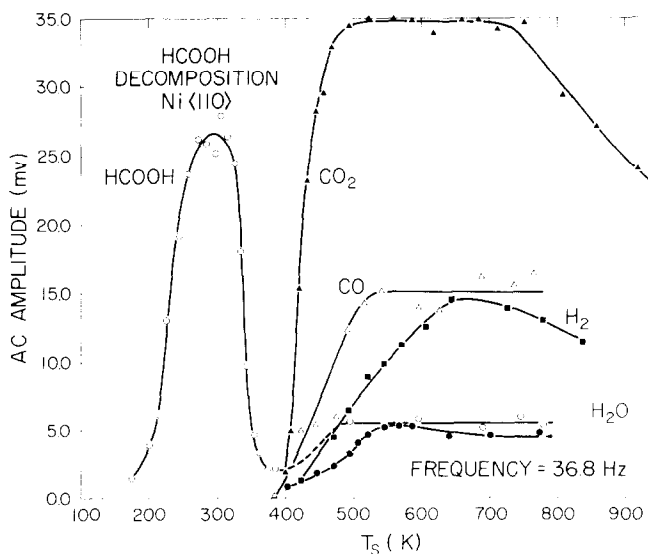


Fig. 4. Amplitudes of the lock-in detector signals for HCOOH and its decomposition products versus surface temperature.

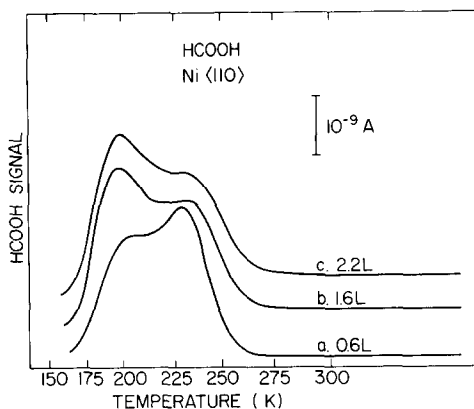


Fig. 5. HCOOH flash desorption spectra following HCOOH adsorption at 150 K.

with peak temperatures of approximately 197 and 231 K as shown in fig. 5. In addition a third binding state leading to decomposition was observed at 390 K for HCOOH on Ni(110) [9]. Presumably, this corresponded to a chemisorbed state while the two desorption peaks observed in this work corresponded to physisorbed states. The peak at 231 K agrees with that observed previously for adsorption at 200 K [18]. The flash desorption results reveal that the adsorption–desorption of HCOOH from the Ni(110) surface was certainly not a simple first-order process and that below room temperature the surface was saturated with reaction intermediates.

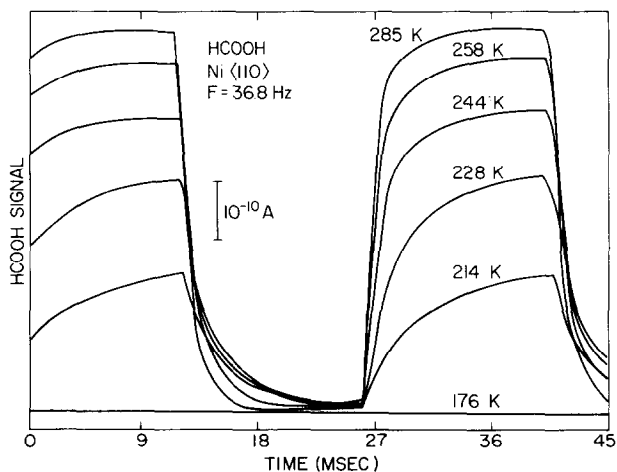


Fig. 6. Smoothed waveforms for the desorption of formic acid from the Ni(110) surface below room temperature.

The smoothed relaxation curves obtained from the waveform eductor for the scattering of HCOOH from the Ni(110) surface below room temperature are shown in fig. 6. The low temperature waveforms show no reflected portion and, therefore, the adsorption probability of formic acid on Ni(110) was unity (see fig. 3 and corresponding discussion). Both the MBRS and flash desorption experiments indicated large surface residence times for the formic acid molecules for surface temperatures below 175 K. The waveforms obtained above room temperature are presented in fig. 7; the response was fast, indicating a short surface residence time above room temperature, and the decomposition probability rapidly increased from zero to 0.90 between 300 and 400 K.

An Arrhenius plot of the apparent first-order rate constant for the desorption of HCOOH from the Ni(110) surface revealed interesting features as shown by fig. 8a. The rate constants were calculated both from the exponential decay of the HCOOH relaxation curves of fig. 6 and from the lock-in phase-lag data. At temperatures below 280 K the Arrhenius plot was linear, but between 280 and 350 K the apparent relaxation time for desorption increased above that expected from the extrapolated adsorption-desorption behavior observed at lower temperatures. This behavior suggested that above 280 K more than one step was governing the interaction of HCOOH with the surface prior to desorption.

The apparent rate constant for the desorption of HCOOH from Ni(110) was calculated from the data in the low temperature range to be:

$$k_0 = 1.6 \times 10^5 \exp(-2.7 \text{ kcal/mol}/RT) \text{ sec}^{-1} . \quad (27)$$

The amplitude behavior of the formic acid signal was back-calculated from the

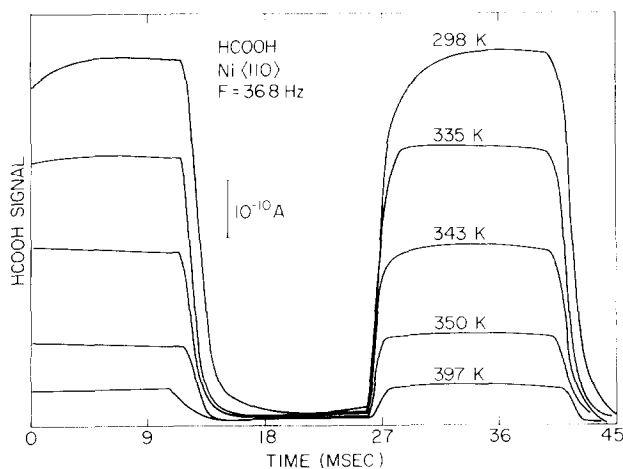


Fig. 7. Smoothed waveforms for the desorption of formic acid from the Ni(110) surface above room temperature.

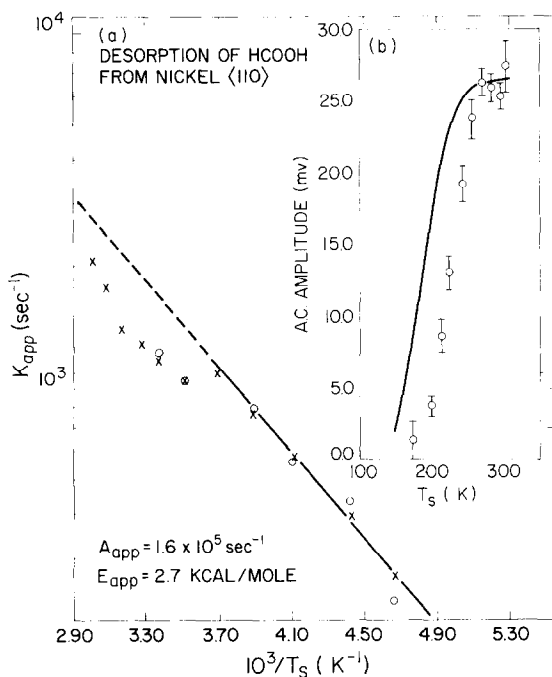


Fig. 8. (a) The apparent first-order rate constant for the desorption of formic acid molecules from the Ni(110) surface; (X) calculated from the lock-in phase-lag data; (O) calculated from the exponential decay of the formic acid waveforms shown in fig. 6. (b) HCOOH ac amplitude below room temperature; (O) obtained from the lock-in detector; (—) calculated from the HCOOH phase-lag data assuming a first-order desorption process.

phase-lag data, assuming *first-order desorption* and was compared to the experimental results as shown in fig. 8b. The lack of exact agreement between the calculated amplitude and the experimental results further demonstrated that *the desorption of HCOOH from the Ni(110) surface was more complex than a simple first-order process.*

4.2. CO_2/HCOOH

The process for the decomposition of HCOOH to produce CO_2 was a linear mechanism and exhibited a change in selectivity away from the production of CO_2 above 700 K. The amplitude and phase behavior of products CO_2 are shown in figs. 4 and 9. The amplitude and phase-lag behavior of the CO_2 signal above surface temperatures of 700 K was consistent with a linear surface process that was undergoing a change in selectivity, since at these high temperatures the amplitude of the CO_2

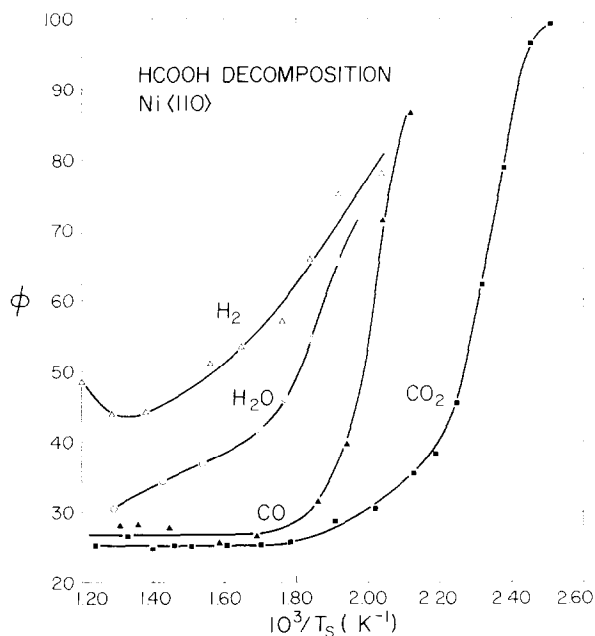


Fig. 9. Phase-lags of the HCOOH decomposition products versus reciprocal surface temperature.

signal substantially decreased, but the phase-lag remained unchanged. A non-linear process, i.e. second-order, would show a simultaneous increase in phase-lag if the surface concentration of the intermediate preceding the product was reduced due to selectivity. Supporting evidence for the linearity of the mechanism producing CO₂ was also obtained when two different isotopes of formic acid were used, DCOOH and HCOOH, at two different beam intensities with $I_{\text{HCOOH}}/I_{\text{DCOOH}} \sim 1.5$; the surface residence time of CO₂ was independent of the isotope and the beam intensity.

The formation of CO₂ occurred by a series mechanism, since phase-lags greater than 90° with respect to reflected HCOOH were observed. Previous characterization of the Ni(110) and the Ni(110) (4 × 5)C surfaces showed that CO₂ formation was not desorption limited at these temperatures [9,19]. Therefore, the CO₂ phase-lag contained information about the decomposition step and the preceding surface processes. At high temperatures the phase-lags of CO₂, CO, and H₂O approached the same limiting value; this suggested that the constant phase-lag of 25.4° was due to a process preceding the decomposition of HCOOH. It is important to note that the surface residence time for the desorbed formic acid was negligible above room temperature (see fig. 8); the phase-lag at the same modulation frequency was only a few degrees. Phase-lag saturation in the vicinity of 25.4° has previously been reported for bulk diffusion processes [4] and branched processes [16]. A bulk diffusion pro-

cess could not have occurred on the Ni(110) single-crystal employed here, and the constant phase-lag at these temperatures was the result of either a process in series with no activation energy or parallel routes to different adsorption sites available to HCOOH prior to decomposition. Since the catalyst surface contained sites covered with oxygen and carbon more than one pathway was certainly possible. Calculations [20] have shown that two competing reactions producing the same product may lead to a sluggish phase-lag which may be relatively constant over a wide range of temperatures or frequency. In order for the apparent activation energy to be zero, however, these steps must be unactivated or the relative phases and amplitudes of each parallel route must change so as to produce no net change in the phase of the resultant product vector. This effect seems unlikely for the 275° range over which $\phi_{\text{CO}_2} = 25.4^\circ$. It thus appears more likely an unactivated step with an apparent frequency factor of approximately 10^3 sec^{-1} . The significance of this value is not understood at this time.

The first-order rate constant for the decomposition of HCOOH to produce CO₂

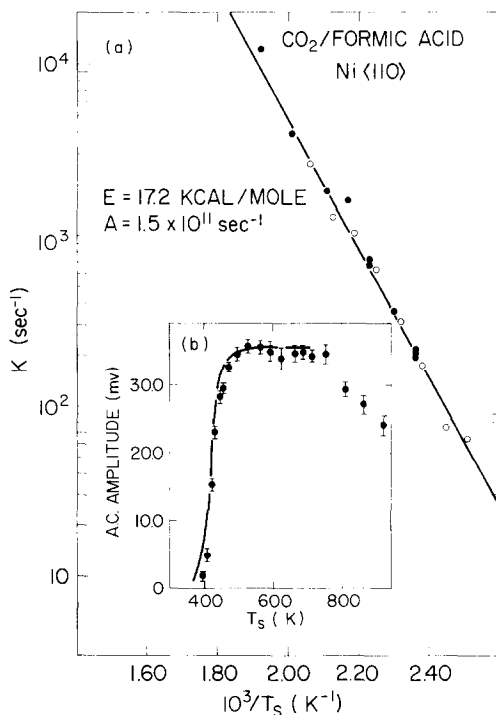


Fig. 10. (a) First-order rate constant for the formation of CO₂ from the decomposition of formic acid; (●) CO₂/HCOOH; (○) CO₂/DCOOH; (b) ac amplitude of product CO₂ versus surface temperature; (●) experimentally obtained with lock-in detector; (—) calculated from the first-order rate constant for the formation of CO₂.

was calculated from the residual phase-lag, $\phi_{r,CO_2} = \phi_{CO_2} - 25.4^\circ$, and was found to be

$$k_2 = 1.50 \times 10^{11} \exp(-17.2 \text{ kcal/mole}/RT) \text{ sec}^{-1}. \quad (28)$$

This rate constant was plotted in fig. 10a with the experimental data. Fig. 10b shows the excellent agreement that resulted when the above rate constant and eq. (17) were used to calculate the amplitude behavior of the CO_2 signal. This calculation did not, of course, predict the change in selectivity observed above 700 K.

4.3. $CO/HCOOH$

The formation of CO from the decomposition of formic acid on a Ni(110) surface was shown by flash desorption to be desorption limited [9]. This deduction is also in agreement with the greater CO phase-lags as compared to CO_2 (fig. 9) observed in this study. Assuming that CO and CO_2 had identical rates of formation, the additional time spent on the surface by CO relative to CO_2 , $\phi_{CO} - \phi_{CO_2}$,

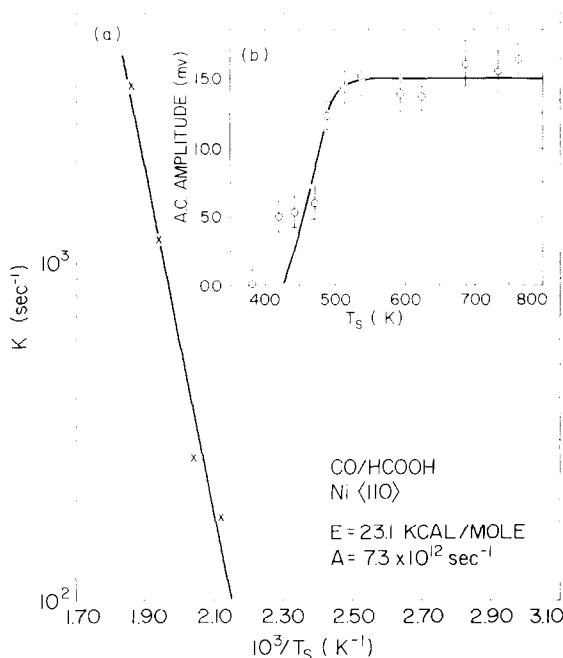


Fig. 11. (a) First-order rate constant for the desorption of CO; (x) calculated from the lock-in phase-lag data; (b) ac amplitude of product CO signal as a function of the surface temperature; (o) experimentally obtained with lock-in detector; (—) calculated from the equations for a series process, the first-order rate constant for the decomposition of HCOOH, and the first-order rate constant for the desorption of CO.

reflects the time necessary for the subsequent desorption of CO. The rate constant for the desorption of CO from the surface was thus calculated from the additional phase-lag and was found to be

$$k_3 = 7.3 \times 10^{12} \exp(-23.1 \text{ kcal/mole}/RT) \text{ sec}^{-1} . \quad (29)$$

The rate constant is plotted in an Arrhenius fashion in fig. 11a with the experimental data. The amplitude curve in fig. 11b was calculated from the rate constant for the decomposition of HCOOH, k_2 , the rate constant for the desorption of CO, k_3 , and the equation for a series process. The rate constant for the desorption of CO was also calculated from the difference in the CO phase-lag and the high temperature phase-lag saturation of 25.4° ; the pre-exponential factor resulting from this calculation was lower by about one-third and the activation energy was lower by about 1 kcal/mole than the values for k_3 reported above. The rate constant was essentially the same for either calculation. Prior to calculation of the above rate constant the CO phase-lag was corrected for cracking contributions from CO_2 and HCOOH in the mass spectrometer; the corrections were 12% and 6.4%, respectively.

4.4. H_2/HCOOH

The larger H_2 phase-lags relative to the CO_2 phase-lags (fig. 9) were attributable to an additional process subsequent to the decomposition of HCOOH; the calculated rate constant and the phase-lag behavior suggested that the additional phase-lag was due to a second-order surface process that occurred subsequent to the decomposition of HCOOH. The second-order rate constant for the recombination of H atoms to form H_2 was also calculated from the difference in the H_2 and CO_2 phase lags, $\phi = \phi_{\text{H}_2} - \phi_{\text{CO}_2}$. The solution for the H_2 phase-lag revealed that this procedure was a valid approximation for the non-linear formation of H_2 when (a) H_2O formation was minor relative to H_2 formation and (b) the adsorption of HCOOH was irreversible. The kinetic data showed that both of these conditions prevailed above room temperature: HCOOH selectively decomposed to form more CO_2 and H_2 than CO and H_2O (as will be discussed below), and the HCOOH signal was greatly diminished at elevated temperatures (see fig. 4). Since the recombination step was second-order, the change in selectivity in the vicinity of 700 K affected the phase-lag data, as shown in fig. 12a. Therefore, only the phase-lag data below 700 K was used. From this data, taking $s_0 = 1.0$ and $I_0 = 10^{13}$ molecules/ cm^2sec , the second-order rate constant for the recombination of H atoms was calculated to be

$$k_5 = 1 \times 10^{-5} \exp(-8.3 \text{ kcal/mole}/RT) \text{ cm}^2/\text{sec} . \quad (30)$$

Fig. 12b compares the calculated amplitude of H_2 with that obtained experimentally. The amplitude behavior of the H_2 signal was reconstructed from the rate constant for the decomposition of HCOOH, k_2 , the above second-order rate constant for the recombination step, and the equation for a second-order process in series with a first-order process. The calculated curve shows the behavior that would have been observed had no change in selectivity occurred above 700 K.

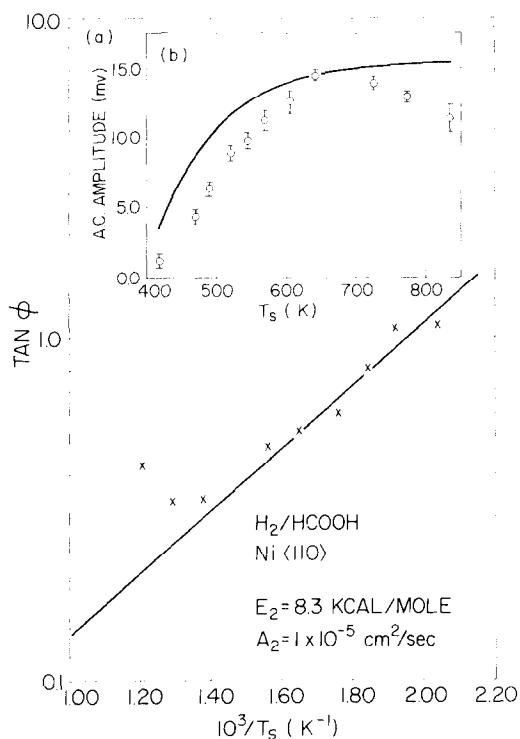


Fig. 12. (a) Second-order rate constant for the recombination step in the formation of H_2 subsequent to the decomposition of $HCOOH$; (x) calculated from the phase-lag data; (b) ac amplitude of product H_2 versus surface temperature; (o) experimentally obtained from lock-in detector; (x) calculated from the equations for a series process, the first-order rate constant for the decomposition of $HCOOH$, and the second-order rate constant of the recombination step subsequent to the decomposition of $HCOOH$.

4.5. $H_2O/HCOOH$

The phase-lag of the H_2O signal was also greater than the phase-lags for the CO_2 and CO signals (fig. 9). Since the desorption time for H_2O from a clean $Ni(110)$ surface was less than 0.1 msec at 500 K [19] the desorption step was not responsible for the additional surface residence time, but another slow process must have followed the decomposition step. The temperature dependence of the phase-lag data, presented below, verified that H_2O was formed by only one slow step subsequent to the decomposition of $HCOOH$; and the rate constant calculated for this step suggested a second-order recombination process for the formation of H_2O .

The second-order rate constant associated with the recombination step was obtained from the difference in the H_2O and CO_2 phase-lags, $\phi = \phi_{H_2O} - \phi_{CO_2}$. As shown in fig. 13a the linearity of $\ln(\tan \phi)$ versus inverse temperature suggested that

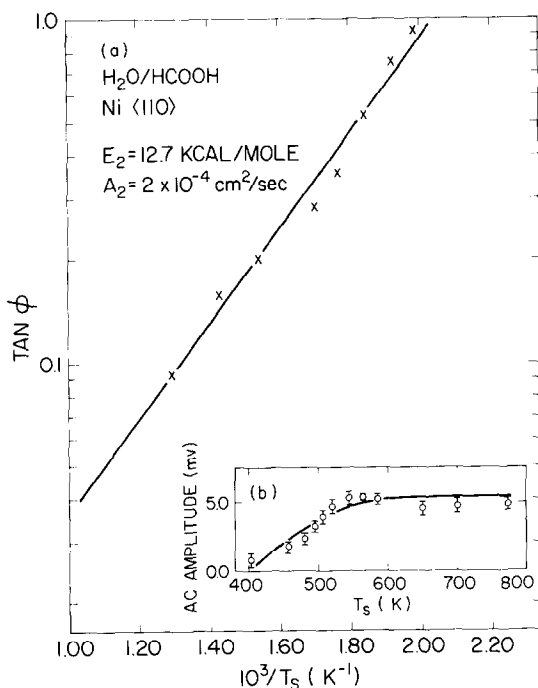


Fig. 13. (a) Second-order rate constant for the formation of H_2O subsequent to the decomposition of HCOOH ; (x) calculated from the phase-lag data; (b) ac amplitude of product H_2O as a function of surface temperature; (o) experimentally obtained from lock-in detector; (—) calculated from the equations for a series process, the first-order rate constant for the decomposition of HCOOH , and the second-order rate constant for the recombination step involved in the formation of H_2O .

only one additional slow step to form H_2O followed the decomposition step to form CO_2 . The phase-lag data, however, does not provide direct information about the intermediates and the exact mechanism of the recombination step. In order to estimate the second-order rate constant, eqs. (11) and (12) were modified because they were only valid when both reacting species existed in equal concentrations on the catalyst surface. The selectivity of HCOOH decomposition for CO_2/CO production was estimated to be about 2.5 from mass spectrometer sensitivities. For this value of the selectivity the corresponding supply rate of H/OH from their respective reaction channels (see eqs. (22) and (23)) was about six. The radicals H and OH are only intended to be representative of the actual intermediates involved. The rate of water formation is given by:

$$R_{\text{H}_2\text{O}} = k_4 n_{\text{H}} n_{\text{OH}}, \quad (31)$$

where k_4 is the second-order rate constant for recombination, and n_{H} and n_{OH} are, respectively, the surface concentrations of H and OH . Since the surface residence

times for H_2 and H_2O were similar ($\phi_{H_2} - \phi_{H_2O} < 15^\circ$ below 800 K), $n_H \sim 6n_{OH}$, to a first-order approximation

$$R_{H_2O} \approx 6k_4 n_{OH}^2. \quad (32)$$

The results now obtained are identical to eqs. (11) and (12), except that the second-order rate constant is replaced by $6k_4$. This derivation assumed that the formation of H_2 and H_2O were not coupled. The second-order recombination rate constant was calculated from fig. 13a, taking $s_0 = 1.0$ and $I_0 = 10^{13}$ molecules/cm²sec, and was found to be

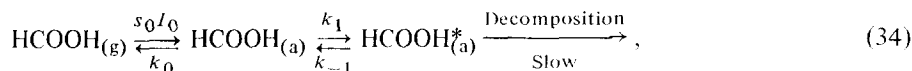
$$k_4 = 2 \times 10^{-4} \exp[-12.7 \text{ kcal/mole}/RT] \text{ cm}^2/\text{sec}. \quad (33)$$

It will be shown below that the above pre-exponential is consistent with a second-order surface process. The amplitude behavior of the H_2O signal was calculated from the proposed series mechanism, and the expressions obtained for k_2 , the decomposition of $HCOOH$, and k_4 , the recombination step in the formation of H_2O . Fig. 13b shows the good agreement obtained between the theoretical amplitude and the actual experimental results. The solution of the H_2O phase-lag was also calculated after making the same approximations as in the derivation of the H_2 phase-lag. Under these circumstances the calculated pre-exponential factor was essentially the same and the activation energy was reduced by about 2 kcal/mole. The good agreement between both approaches further substantiate the approximations that were made in both derivations. Before the above calculation was performed the H_2O signal was corrected for an 8% cracking contribution from $HCOOH$.

5. Discussion

5.1. Adsorption-desorption of $HCOOH$

The apparent rate-constant for the desorption of $HCOOH$ shown in fig. 8a deviated from simple first-order Arrhenius behavior at approximately the same temperature where the onset of formic acid decomposition was observed. Therefore, it appeared that the desorption and decomposition of formic acid were coupled; had decomposition and desorption occurred independently, the deviation from linearity would not have been observed. This behavior suggested that there existed a precursor state to decomposition. The influence of the precursor state is represented by the following series mechanism



where $HCOOH_{(a)}^*$ is the precursor to decomposition, k_0 is the rate constant for desorption, and k_1 and k_{-1} are the rate constants for supplying and removing formic

acid from the precursor state, respectively. $\text{HCOOH}_{(a)}^*$ is taken to represent the chemisorbed formic acid, and $\text{HCOOH}_{(a)}$ represents the loosely bound physisorbed formic acid. Below room temperature the surface was saturated with chemisorbed formic acid and the rate of decomposition was too slow to be significant. The phase-lag for the desorption of HCOOH according to this mechanism was found to be [13]

$$\phi = \tan^{-1} \frac{\omega[k_{-1}(k_1 + k_{-1}) + \omega^2]}{k_{-1}^2 k_0 + (k_0 + k_1)\omega^2} . \quad (35)$$

Since the phase-lag can also be represented by

$$\phi = \tan^{-1} (\omega/K_{\text{app}}) , \quad (36)$$

the apparent rate constant is given by the expression:

$$K_{\text{app}} = \frac{k_{-1}^2 k_0 + (k_0 + k_1)\omega^2}{k_{-1}(k_1 + k_{-1}) + \omega^2} . \quad (37)$$

The above mechanism qualitatively accounts for the observed behavior of formic acid desorption. Below 280 K, the temperature regime where $\ln K_{\text{app}}$ was linear with $1/T$, access to and from the precursor state was limited, $k_1 \approx k_{-1} \approx 0$, and

$$K_{\text{app}} = k_0 . \quad (38)$$

At higher temperatures ($T_s > 280$ K) both k_1 and k_{-1} were greater than ω , and under these circumstances

$$K_{\text{app}} \leq k_0 . \quad (39)$$

The apparent desorption rate constant would thus be expected to fall below k_0 when the reaction channel to the precursor opened and return to the value expected for desorption, k_0 , when the decomposition became rapid. Fig. 8a shows these qualitative features. It is important to note that according to eq. (14), the magnitude of the pre-exponential factor observed indicated a second-order desorption step (assuming $s_0 = 1$, $I_0 = 10^{13}$ molecules/cm² sec, $\epsilon = \infty$, yielded $A_2 = 10^{-3}$ cm²/sec). We are examining this point further.

5.2. CO_2/HCOOH

The change in selectivity away from the formation of product CO_2 above 700 K was probably due to the changing surface concentration of oxygen. Above surface temperatures of 700 K the amplitude of the CO_2 signal decreased; the steady-state coverage of oxygen on Ni(110) also decreased at these same temperatures (see table 1). More recent results have shown that the product selectivity CO_2/CO was about 3 on an oxygen covered Ni(110) [21] surface compared to $\text{CO}_2/\text{CO} \sim 1.0$ on the

clean Ni(110) surface [9]. In agreement with those results we observed the selectivity of $\text{CO}_2/\text{CO} \sim 2.5$ below 700 K, when one-third monolayer of oxygen was present. The investigation on the oxygen covered Ni(110) surface mentioned above utilized isotopes of oxygen to ensure that C^{16}O did not react with the adsorbed oxygen to yield $\text{C}^{16}\text{O}^{18}\text{O}$.

The first-order pre-exponential factor of $1.5 \times 10^{11} \text{ sec}^{-1}$ obtained by MBRS for the formation of CO_2 from the decomposition of HCOOH was substantially less than $1.6 \times 10^{15} \text{ sec}^{-1}$ reported for the explosive flash decomposition of DCOOH on clean Ni(110) [6]. The explosive mechanism occurred only at surface coverages above $\theta = 0.1$, while above room temperature the molecular beam produced a surface concentration $\theta \sim 10^{-3} - 10^{-4}$. At low surface coverages ($\theta < 0.1$) the flash decomposition of formic acid was not explosive and the first-order rate constant was found to be [22] $4 \times 10^{15} \exp(-25.0 \text{ kcal/mole}/RT) \text{ sec}^{-1}$. In addition, on a Ni(110) surface exposed to 1 Langmuir of oxygen the decomposition of formic acid occurred via both autocatalytic and first-order mechanisms; the rate constants were $4.0 \times 10^{11} \exp(-20.8 \text{ kcal/mole}/RT) \text{ sec}^{-1}$ and $1.7 \times 10^{12} \exp(-21.5 \text{ kcal/mole}/RT) \text{ sec}^{-1}$, respectively [21]. On the Ni(110) (2 × 1)C surface the first-order rate constant was observed to be $2 \times 10^{12} \exp(-25.0 \text{ kcal/mole}/RT) \text{ sec}^{-1}$ [23]. The magnitude of the pre-exponential factor for decomposition on the oxide or the carbide surface is in good agreement with that observed here. Using the formalism of transition state theory the low pre-exponential factor reported here implies either a loosely bound precursor state or a transition state having little freedom of motion. It may be possible that under identical experimental conditions both types of experiments, flash desorption and MBRS, will yield the same results. It does appear, however, that the intermediates and/or the transition states formed at low and high coverages do differ.

The rate constants presented above for the formation of CO_2 from the flash decomposition of formic acid on the Ni(110) clean, carbide, and oxide surfaces were incorporated in a hypothetical parallel reaction mechanism. The model assumed that CO_2 was simultaneously produced on bare nickel sites, oxygen covered nickel sites, and carbon covered nickel sites. The equations for a parallel mechanism (eqs. (5), (6), (9), and (10)) were used to generate the phase-lag behavior. All possible permutations of rate constants and branching probabilities were examined and *none of the results reproduced the CO_2 phase-lag behavior of fig. 9*. This simulation further suggested that the process responsible for the phase-saturation of 25.4° preceded the decomposition of HCOOH .

5.3. CO/HCOOH

The CO desorption rate constant, $7.3 \times 10^{12} \exp[-23.1 \text{ kcal/mole}/RT] \text{ sec}^{-1}$, was observed to be in excellent agreement with the data for desorption of CO from a carburized Ni(110) surface [19], $2 \times 10^{12} \exp[-21.0 \text{ kcal/mole}/RT] \text{ sec}^{-1}$. The rate constants for the desorption of CO from a clean Ni(110) [24] surface, $8.5 \times$

$10^{15} \exp[-32.7 \text{ kcal/mole}/RT] \text{sec}^{-1}$, and an oxygen covered surface [21], $2 \times 10^{16} \exp[-25.5 \text{ kcal/mole}/RT] \text{sec}^{-1}$, were substantially different than the rate constant obtained in this study. The CO data that was used to calculate the above desorption rate constant corresponded to the temperature regime where the steady-state surface coverages of carbon and oxygen were at their maximum. It is not apparent why the rate constant for the desorption of CO was similar to that for desorption from a carbide surface, unless CO preferentially desorbed from the carbide overlayer.

5.4. $\text{H}_2\text{O}/\text{HCOOH}$ and H_2/HCOOH

The amplitude behavior of H_2 calculated from the phase data was only in fair agreement with the experimentally obtained data for temperatures less than 700 K. In the calculations it was assumed that the influence of background hydrogen was negligible, the equations for the formation of H_2 were not coupled with those for H_2O formation, and the adsorption of HCOOH was irreversible. Since the calculated curve lay above the experimental data the actual activation energy may have been about 2–3 kcal/mole larger than that calculated; a larger activation energy results in a slightly larger pre-exponential factor.

The calculated curve for the behavior of the H_2O amplitude was in good agreement with the experimental data, further indicating that the approximations introduced in the derivation of eq. (32) were reasonable. The two derivations utilized neglected the possibility of surface oxygen reacting with H atoms to produce H_2O . The significance of this step was difficult to assess and it was, therefore, omitted for simplicity.

The second-order pre-exponential factor, $\nu_0^{(2)}$, has been estimated from the frequency of collisions of a two-dimensional gas on the surface and the hopping model of surface diffusion. The collision frequency of a two-dimensional gas is described by [25]:

$$\nu_0^{(2)} = \sigma_0(\pi kT/m)^{1/2}, \quad (40)$$

where σ_0 is the hard-sphere collision diameter, k is the Boltzmann constant, and m is the mass of the particle. The hopping model yields a different expression for the second-order pre-exponential [25]

$$\nu_0^{(2)} = a^2 \nu_0, \quad (41)$$

where a is the jump length and ν_0 is the vibrational frequency of an adsorbed atom (usually taken as 10^{13} sec^{-1}). Typical second-order pre-exponentials obtained from these models, for the recombination of hydrogen atoms, are $\nu_0^{(2)} = 10^{-3} - 10^{-1} \text{ cm}^2/\text{sec}$. Both models assume that hydrogen atoms are the only surface species, do not account for interactions between different types of surface species, and neglect adsorbate–substrate interactions.

The second-order pre-exponentials calculated for the formation of H_2 (1×10^{-5}

cm^2/sec) and H_2O ($2 \times 10^{-4} \text{ cm}^2/\text{sec}$) are much smaller than predicted by either of the two models discussed above. Using the formalism of transition state theory this may indicate that the probability of reactants in proper configuration in phase space to form products is low because of inefficient energy transfer with the surface to stabilize the intermediate, or there may exist a stringent requirement on the trajectories of the colliding partners to collide with an appreciable normal component (as was originally suggested [26] as an explanation for the non-diffusive desorption of HD from nickel). Other investigators have also observed low values for the second-order pre-exponential factor for the desorption of D_2 from Ni(110) (2×10^4) [27]. This phenomenon may be quite general, particularly for desorption of gases from surface chemilayers containing carbon, oxygen or sulfur, for example.

6. Summary and conclusion

The results presented showed that the onset of formic acid decomposition occurred in the vicinity of 300 K on the Ni(110) surface. Below 280 K the apparent rate constant for the desorption of formic acid exhibited linear behavior and formic acid desorbed from a Ni(110) surface saturated with chemisorbed formic acid; this is represented by step (19). Above 280 K an additional "channel" opened up for the adsorbed HCOOH, step (20). The evidence for this step was the additional surface residence time of HCOOH above 280 K. At elevated temperatures the surface coverage of formic acid intermediates was extremely low and formic acid adsorbed upon a Ni(110) surface partially covered with carbon and oxygen. The overall selectivity for the decomposition of HCOOH was determined by the competition between the dissociation steps (22) and (23) and was calculated to be $P = 0.71$ below 700 K.

This study demonstrates the ability of MBRS to probe the details of the kinetics that occur on solid surfaces. The rate constants for the desorption of HCOOH, decomposition of HCOOH, desorption of CO, and the recombination steps involved in the formation of H_2 and H_2O on Ni(110) were calculated. The second-order rate constants for H_2 and H_2O formation indicated severe steric limitations, possibly due to the necessity of stabilizing energy transfer to the solid upon desorption. Additional insight into the surface kinetics was obtained by AES analysis of the steady-state surface coverage at a series of temperatures. The temperature dependence of the steady-state surface coverage accounted for the change in CO_2 production above 700 K and the hysteresis effect. The mechanism observed for the decomposition of HCOOH on Ni(110) with overlayers of carbon and oxygen with MBRS at low coverages was different than the explosive decomposition of HCOOH obtained with flash desorption spectrometry on clean Ni(110) at high coverages.

Appendix. The analytical solution of the product phase-lags

The phase-lags of the various reaction products were directly calculated by methods previously presented in the literature [13,17]. The product phase-lags were obtained by performing mass balances on the five distinct surface species ($\text{HCOOH}_{(a)}$, $\text{HCOOH}^*_{(a)}$, $\text{CO}_{(a)}$, $\text{H}_{(a)}$, $\text{OH}_{(a)}$) presented in eqs. (21) to (26)

$$dn_{\text{HCOOH}}/dt = s_0 J_{0g}(t) - k'_1 n_{\text{HCOOH}}, \quad (42)$$

$$dn_{\text{HCOOH}^*}/dt = k'_1 n_{\text{HCOOH}} - k_2 n_{\text{HCOOH}^*}, \quad (43)$$

$$dn_{\text{CO}}/dt = k_2(1 - P)n_{\text{HCOOH}^*} - k_3 n_{\text{CO}}, \quad (44)$$

$$dn_{\text{H}}/dt = k_2(1 + P)n_{\text{HCOOH}^*} - k_4 n_{\text{H}} n_{\text{OH}} - k_5 n_{\text{H}}^2, \quad (45)$$

$$dn_{\text{OH}}/dt = k_2(1 - P)n_{\text{HCOOH}^*} - k_4 n_{\text{H}} n_{\text{OH}}. \quad (46)$$

The waveforms for HCOOH showed that the adsorption of HCOOH was complete and essentially irreversible above room temperature. The constancy of the phase-lag for reaction products at high temperatures strongly suggested that an unactivated process preceded the formation of HCOOH^* ; this is represented by the rate constant k'_1 . At the modulation frequency employed this process could not be further analyzed. Consequently, all reaction processes were analyzed subsequent to this step, and the phase-lag due to this process was subtracted out. This treatment must be considered as the best approximation available at this time.

The phase-lags of the formic acid reaction products were directly obtained by simultaneously solving the differential equations (42) to (46). The only assumption made in the derivation was that H_2O formation was minor relative to H_2 formation. With this constraint the product phase-lags were expressed by:

$$\phi_{\text{CO}_2} = \tan^{-1}(\omega/k'_1) + \tan^{-1}(\omega/k_2), \quad (47)$$

$$\phi_{\text{CO}} = \tan^{-1}(\omega/k'_1) + \tan^{-1}(\omega/k_2) + \tan^{-1}(\omega/k_3), \quad (48)$$

$$\phi_{\text{H}_2} = \tan^{-1}(\omega/k'_1) + \tan^{-1}(\omega/k_2) + \tan^{-1}(\omega/K_{\text{H}_2}), \quad (49)$$

$$\begin{aligned} \phi_{\text{H}_2\text{O}} = & \tan^{-1}(\omega/k'_1) + \tan^{-1}(\omega/k_2) \\ & + \tan^{-1} \frac{\omega}{K_{\text{H}_2}} \frac{k_5}{k_4} \frac{1 + 2(\omega/K_{\text{H}_2})^2(1 + k_5/k_4)}{1 + (\omega/K_{\text{H}_2})^2[3(k_5/k_4) + 2(k_5/k_4)^2 + 1]}, \end{aligned} \quad (50)$$

where

$$K_{\text{H}_2} = [2(1 + P)s_0 J_0 k_5]^{1/2}. \quad (51)$$

Note that K_{H_2} is identical to the apparent rate constant for a second-order surface process (see eqs. (13) to (15) and table 2).

Eqs. (47) to (49) reveal that the difference in the phase-lags of the products were related to the rate constants for the decomposition of $HCOOH$, k_2 , the desorption of CO , k_3 , and the recombination of H atoms, k_5 :

$$\phi_{CO_2} - 25.4^\circ = \tan^{-1} (\omega/k_2), \quad (52)$$

$$\phi_{CO} - \phi_{CO_2} = \tan^{-1} (\omega/k_3), \quad (53)$$

$$\phi_{H_2} - \phi_{CO_2} = \tan^{-1} (\omega/K_{H_2}). \quad (54)$$

The difference $\phi_{H_2O} - \phi_{CO_2}$ did not reduce to a simple expression, but since our experimental results demonstrated that $(\omega/K_{H_2})^2 < 1$ over a wide temperature range (see fig. 12)

$$\phi_{H_2O} - \phi_{CO_2} \approx \tan^{-1} \left(\frac{\omega}{K_{H_2}} \frac{k_5}{k_4} \right). \quad (55)$$

This analysis demonstrated that under certain constraints the elementary kinetic parameters can be directly obtained from the differences in the product phase-lags.

References

- [1] R.J. Madix and J.A. Schwarz, *Surface Sci.* 24 (1971) 264.
- [2] J.A. Schwarz and R.J. Madix, *Surface Sci.* 46 (1974) 317.
- [3] D.R. Olander, W. Siekhaus, R. Jones and J.A. Schwarz, *J. Chem. Phys.* 57 (1972) 408.
- [4] D.R. Olander, R.H. Jones, J.A. Schwarz and W.J. Siekhaus, *J. Chem. Phys.* 57 (1972) 421.
- [5] R.L. Palmer, *J. Vacuum Sci. Technol.* 12 (1975) 1403.
- [6] J.L. Falconer and R.J. Madix, *Surface Sci.* 46 (1974) 473.
- [7] R.J. Madix, J. Falconer and J. McCarty, *J. Catalysis* 31 (1973) 316.
- [8] J. Falconer, J. McCarty and R.J. Madix, *Japan. J. Appl. Phys. Suppl.* 2 Pt. 2 (1974) 525.
- [9] J. McCarty, J. Falconer and R.J. Madix, *J. Catalysis* 30 (1973) 235.
- [10] J. McCarty, Ph.D. Dissertation, Stanford University (1974).
- [11] T.N. Taylor and P.J. Estrup, *J. Vacuum Sci. Technol.* 10 (1973) 26.
- [12] D.R. Olander, in: *The Structure and Chemistry of Solid Surfaces*, Ed. G.A. Somorjai (Wiley, New York, 1969) p. 45-1.
- [13] R.H. Jones, D.R. Olander, W.J. Siekhaus and J.A. Schwarz, *J. Vacuum Sci. Technol.* 9 (1972) 1429.
- [14] R.J. Madix, *Surface Sci.* 45 (1974) 696.
- [15] C.T. Foxon, M.R. Boudry and B.A. Joyce, *Surface Sci.* 44 (1974) 69.
- [16] S.L. Bernasek and G.A. Somorjai, *J. Chem. Phys.* 62 (1975) 3149.
- [17] D.R. Olander and A.Z. Ullman, *Intern. J. Chem. Kin.* 8 (1976) 625.
- [18] J. Falconer and R.J. Madix, to be published.
- [19] J.G. McCarty and R.J. Madix, *Surface Sci.* 54 (1976) 121.
- [20] R.H. Jones, Ph.D. Dissertation, U.C. Berkeley (1971).

- [21] S.W. Johnson and R.J. Madix, to be published.
- [22] D. Ying and R.J. Madix, to be published.
- [23] J. McCarty and R.J. Madix, *J. Catalysis* 38 (1975) 402.
- [24] J.L. Falconer and R.J. Madix, *Surface Sci.* 48 (1975) 393.
- [25] P.W. Tamm and L.D. Schmidt, *J. Chem. Phys.* 51 (1969) 5352.
- [26] R.L. Palmer, J.N. Smith, Jr., H. Saltsburg and D.R. O'Keefe, *J. Chem. Phys.* 53 (1970) 1666.
- [27] N.M. Abbas and R.J. Madix, *Surface Sci.* 62 (1977) 739.